Structure of follicle-stimulating hormone in complex with the entire ectodomain of its receptor

Xuliang Jiang[a], Heli Liu[b], Xiaoyan Chen[b], Po-Han Chen[b], David Fischer[a], Venkataraman Sriraman[a], Henry N. Yu[a], Steve Arkinstall[a], and Xiaolin He[b,1]

[a]EMD Serono Research Institute, Billerica, MA 01821; and [b]Department of Molecular Pharmacology and Biological Chemistry, Northwestern University Feinberg School of Medicine, Chicago, IL 60611

Edited by Wayne A. Hendrickson, Columbia University, New York, NY, and approved June 22, 2012 (received for review April 25, 2012)

FSH, a glycoprotein hormone, and the FSH receptor (FSHR), a G protein-coupled receptor, play central roles in human reproduction. We report the crystal structure of FSH in complex with the entire extracellular domain of FSHR ($FSHR_{ED}$), including the enigmatic hinge region that is responsible for signal specificity. Surprisingly, the hinge region does not form a separate structural unit as widely anticipated but is part of the integral structure of $FSHR_{ED}$. In addition to the known hormone-binding site, $FSHR_{ED}$ provides interaction sites with the hormone: a sulfotyrosine (sTyr) site in the hinge region consistent with previous studies and a potential exosite resulting from putative receptor trimerization. Our structure, in comparison to others, suggests FSHR interacts with its ligand in two steps: ligand recruitment followed by sTyr recognition. FSH first binds to the high-affinity hormone-binding subdomain of FSHR and reshapes the ligand conformation to form a sTyr-binding pocket. FSHR then inserts its sTyr (i.e., sulfated Tyr335) into the FSH nascent pocket, eventually leading to receptor activation.

sulfated tyrosine recognition | signal transduction | reproductive hormone | leucine-rich repeat | CF3 motif

FSH is a gonadotropin that stimulates steroidogenesis and gametogenesis in the gonads. Secreted by the anterior pituitary gland, FSH regulates the menstrual cycle and ovarian follicular maturation in women and supports sperm production in men. FSH acts by binding to the FSH receptor (FSHR) on the granulosa cell surface in ovaries and the Sertoli cell surface in testes. The stimulated receptor leads to the dissociation of α- and βγ- subunits of G protein heterotrimer inside the cell. The α-subunit activates adenylyl cyclase, resulting in an increase of cAMP levels, and ultimately leads to the increased steroid production that is necessary for follicular growth and ovulation in women. The free βγ dimers recruit G protein-coupled receptor (GPCR) kinases to the receptor, which, in turn, lead to the recruitment of β-arrestin to the receptor (1). FSH is used clinically for controlled ovarian stimulation in women treated with assisted reproductive technologies and also for the treatment of anovulatory infertility in women and hypogonadotropic hypogonadism in men. The central role of FSH in human reproduction makes its receptor a unique pharmaceutical target in the field of fertility regulation (2–4).

The glycoprotein hormone (GPH) family has four members: FSH; two other pituitary hormones, luteinizing hormone and thyroid-stimulating hormone (TSH); and one placental hormone, chorionic gonadotropin. The four members are homologous in sequence, structure, and function. Each member is a heterodimer composed of a common α-subunit and a hormone-specific β-subunit. The crystal structures of FSH and human CG (hCG) revealed that both α- and β-subunits adopt similar folds of cystine-knot architecture (5–7). The assembled α- and β-heterodimers bind to their respective receptors with high affinity and hormone specificity, resulting in similar signaling pathways but distinct biological responses.

The glycoprotein hormone receptors (GPHRs) are members of the GPCR superfamily that transduce extracellular signals into G protein activation through their seven-helical transmembrane domains (1). The GPHRs belong to family A, whose prototypical member is rhodopsin. Unlike other family A GPCRs with short extracellular N-terminal peptide, the GPHRs have unusually large ectodomains that contain 340–420 amino acids in length and bind large ligands with molecular masses around 33 kDa. The large ectodomain has been proposed to contain two functional domains: a rigid hormone-binding domain at the N terminus responsible for the high-affinity ligand recognition (8–10) and an enigmatic juxtamembrane hinge domain responsible for signal specificity (11, 12). The structure model of the hormone-binding region was proposed in the mid-1990s (13). The detailed recognition between the ligand and the N-terminal hormone-binding domain of FSHR ($FSHR_{HB}$) has been revealed in a complex structure by Fan and Hendrickson (8, 14). The structure of the signal-specific domain (i.e., hinge), however, has so far been elusive. In the absence of this domain, it is difficult to understand how the ligand-binding signal is conveyed to the transmembrane domain, and the observed ligand receptor-binding mode was challenged and an alternative mode was proposed (15). It has also been shown that sulfated tyrosines in the hinge region of GPHRs (including Y335 for FSHR) are required for hormone recognition and signaling (16). How sulfated residues interact with the hormones, and subsequently lead to receptor activation, remains poorly understood.

To clarify the role of the hinge region in signal transduction, and to explore the full spectrum of ligand-receptor recognition, we have determined the crystal structure of FSH in complex with the entire ectodomain of $FSHR_{ED}$. Unexpectedly, the hinge region does not form a separate structural unit but is an integral part of $FSHR_{ED}$. Although the primary hormone-binding site agrees with the previous study, $FSHR_{ED}$ provides two additional binding sites for the ligand and these sites are in accordance with previously published functional data. Our data support that the hinge region, which harbors a sulfated tyrosine residue, plays a pivotal role in ligand recognition and signal transduction.

Results and Discussion

Overall Structure of FSH–$FSHR_{ED}$ Complex. We determined the structure of human FSH–$FSHR_{ED}$ complex (Fig. 1) in the P1

Author contributions: X.J. and X.H. designed research; X.J., H.L., X.C., P.-H.C., D.F., V.S., H.N.Y., and X.H. performed research; X.J., S.A., and X.H. analyzed data; and X.J. and X.H. wrote the paper.

Conflict of interest statement: D.F., V.S., H.N.Y., S.A., and X.J. are employees of EMD Serono, Inc., an affiliate of Merck KGaA, Germany, whose commercial products include FSH.

This article is a PNAS Direct Submission.

Data deposition: The atomic coordinates and structural factors have been deposited in the Protein Data Bank, www.pdb.org (PDB ID code 4AY9).

[1]To whom correspondence should be addressed. E-mail: x-he@northwestern.edu.

This article contains supporting information online at www.pnas.org/lookup/suppl/doi:10.1073/pnas.1206643109/-/DCSupplemental.

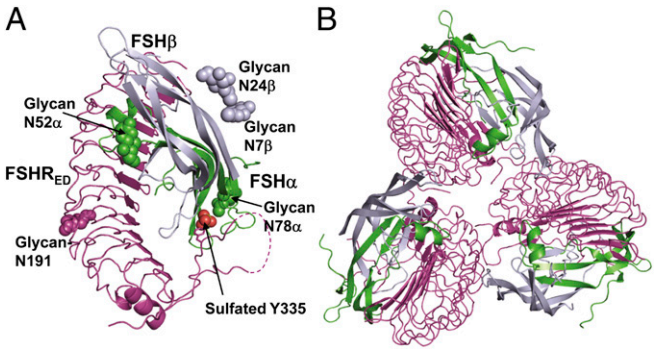

Fig. 1. Structure of human FSH in complex with human FSHR$_{ED}$. (*A*) Ribbon model of human FSH bound to FSHR$_{ED}$: FSH α-subunit is shown in green, FSH β-subunit is shown in purple, and FSHR$_{ED}$ is shown in magenta. The side chain of sulfated Y335 is depicted as sticks for the tyrosine stem and colored balls for the sulfate group. The carbohydrates are depicted as balls. The disordered residues in the receptors are marked as dashed lines. (*B*) Top view of the trimer observed in the asymmetrical unit.

space group at a resolution of 2.5 Å. The overall FSHR$_{ED}$ structure resembles a right hand, with the main body as the palm and the protruding hairpin loop as the thumb. FSHR$_{ED}$ binding to FSH is similar to the right hand holding an American football (Fig. 1*A*). The final structure model contains all residues of FSHR$_{ED}$ except a few disordered ones in the C-terminal region (Tables S1 and S2). Unexpectedly, we observed a trimer in the asymmetrical unit. Although the trimer structure is consistent with some functional data (discussed below), its physiological relevance remains to be determined. In this report, we focus on the structural features and the receptor activation mechanism within one pair of FSH and FSHR.

Hinge Region Is an Integral Part of FSHR$_{ED}$. The hinge region of the GPHRs has been described as "enigmatic" and is expected to be highly flexible and to form a separate structural unit (12, 15, 17, 18). Our structure reveals that the hinge region is not a separate structural unit but, rather, an integral part of the ectodomain (Fig. 2 *A* and *B*). FSHR$_{ED}$ is composed of 12 leucine-rich repeats (LRRs), N- and C-terminal flanking sequences, and a hairpin loop inserted between LRR 11 and LRR 12. The 12 LRRs of the hormone-binding region and the hinge region adopt a continuous geometrically uninterrupted structure, with the inner β-strands gradually steepening their curvature to form a sleigh-like sheet (Fig. S1*B*).

Interestingly, the hinge region contains two peculiar sequence motifs coupled by three disulfide bonds (Fig. 2*B*, *Inset*). The first one includes the residues from L264 to R298 that have been previously identified as motif CF3 specifically existing in GPCR proteins (19). The second one extends from residue Y322 to the last residue R366, right before the first transmembrane domain, which is comparable to the N-terminal extracellular loop of rhodopsin attributable to the analogous intronic luteinizing hormone receptor (LHR) sequences corresponding to the promoter and other regulatory regions of the intronless genes of β-adrenergic receptor and rhodopsin (20, 21). Our structure shows CF3 is tightly linked to the rhodopsin-like extracellular loop at the C-terminal end via three disulfide bonds between C275, C276, and C292 and C346, C356, and C338, respectively, and the disulfide bond pattern is in agreement with an earlier assignment based on mutagenesis experiments (22). At the N-terminal end, CF3 is coupled to the other LRRs through rigid, continuous hydro-

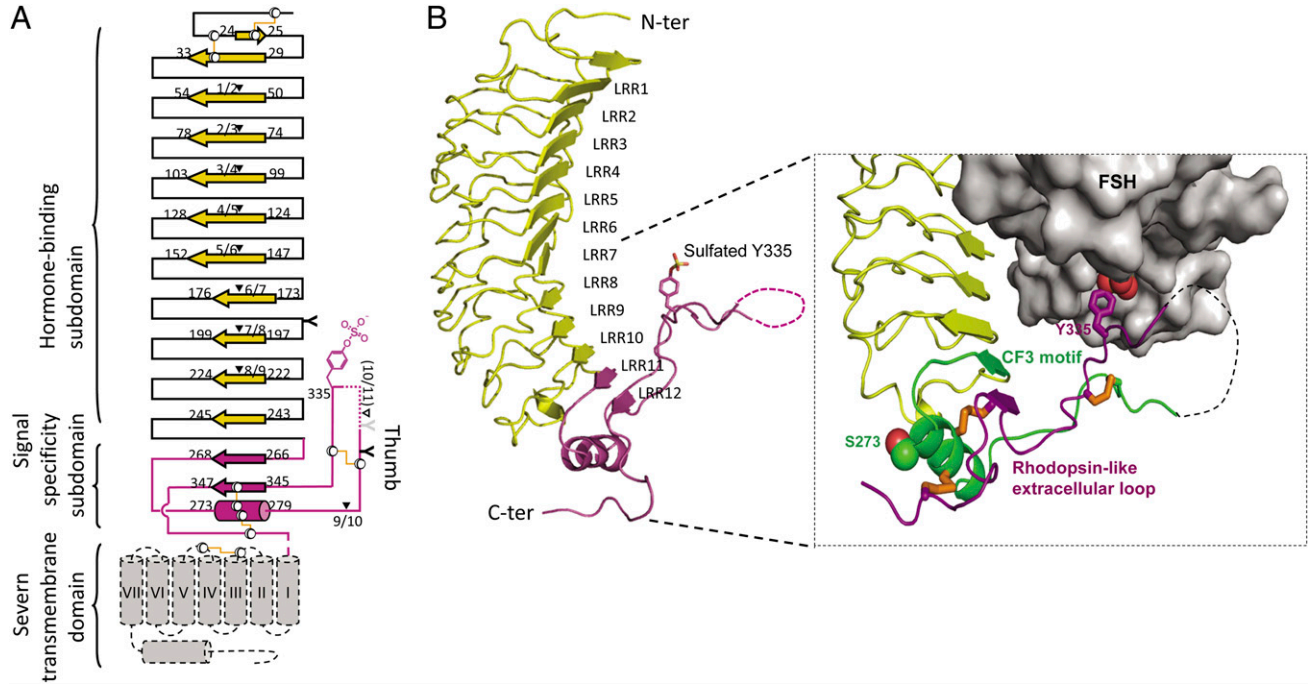

Fig. 2. Structure of FSHR$_{ED}$. (*A*) Schematic diagram of the topology of the FSHR structure. The regular secondary structure elements of LRRs are shown as arrows for the β-strands and as a cylinder for the α-helix. Disulfide bonds are shown as yellow lines linking cysteines, the *N*-linked glycosylation sites are shown as "Y," and the exon boundaries in the FSHR gene are shown as black triangles (▼). (*B*) Ribbon representation of FSHR$_{ED}$. The hormone-binding subdomain is shown in yellow, and the signal specificity subdomain (hinge region) is shown in magenta. (*Inset*) In the close-up view of the signal specificity subdomain, motif CF3 is colored green, the hormone-binding region is colored yellow, and the rhodopsin-like extracellular sequence is colored magenta. The disulfide bonds are shown as brown sticks, sulfated Y335 is shown as sticks for the phenyl ring and balls for the sulfate group, and the side chain of S273 is shown as balls. As a reference, FSH is included as a gray surface.

phobic interactions. Thus, CF3 serves as a bolt to lock the hormone-binding subdomain and the rhodopsin-like extracellular loop together. This suggests that large-scale conformational change within the FSHR extracellular domain ($FSHR_{ED}$) on ligand binding is unlikely, and it does not support earlier proposed models in which the receptor was activated as the result of a significant conformational rearrangement in the hinge region (15, 17, 18).

Sulfotyrosine Site: Insertion of the Sulfated Tyrosine of FSHR into a Nascent FSH Pocket. In addition to the hormone-recognition site at the concave face of the LRR of FSHR as previously reported (8), our structure reveals the detailed hormone-receptor interactions involving sulfated Y335, designated hereafter as the sulfotyrosine (sTyr) site. Each sTyr site buries a 650-$Å^2$ solvent-accessible surface area. The salient feature of this site is the insertion of the sulfated FSHR Y335 into an FSH pocket. The sulfate group forms hydrogen bonds with the terminal amide groups of Q27α and N15α, as well as with the main chain nitrogen atoms of Val38β and Tyr39β at the bottom of the FSH pocket. Lining the wall of the FSH pocket are the hydrophobic residues P16α, L17α, F18α, F74α, L37β, Y39β, and P45β from the loops ℒ1α, ℒ3α, and ℒ2β, as well as the positively charged residue R35 (Fig. 3*A*). The large number of hydrophobic residues creates a low dielectric-constant microenvironment, enhancing Coulomb charge-charge attraction between the FSHR sulfate and FSH R35β aligned on the upper side of the binding pocket, as well as providing a necessary milieu to accommodate the Y335's hydrophobic phenyl ring. Despite the small interaction area at this site, sulfated Y335 is essential for FSHR activation (16, 23). In LHR, the equivalently sulfated tyrosine Y331 and its preceding residue D330 have also been determined as the key signaling residues by site-directed mutagenesis (22). Monoclonal antibody 106-105 bound to native human FSHR against residues at or near this site completely blocked cAMP production (24). Notably, the gonadotropin α-chain mutations Q13K, E14K, P16K, and Q20K turned human TSH into a superagonist (25); these mutations are concentrated near the top right side of the pocket, generating additional positive charges for a stronger anodic potential to pull the rhodopsin-like extracellular loop further to the top right.

To form the recognition pocket to house FSHR's sulfated Y335, FSH changes its conformation dramatically at the sTyr site. Its ℒ2β loop (residues from V38β to Q48β), roughly half of the building block of the pocket, swings ~10 Å from the open and loose conformation in the free form to the closed and rigid conformation in the receptor-bound form (Fig. 4 and Fig. S2). Interestingly, the ℒ2β loop conformation in the previous FSH–$FSHR_{HD}$ complex structure (8), which lacks the hinge region, and hence the sulfated tyrosine, is similar to the ℒ2β loop of our structure but not to the one from the free FSH. This pocket-forming ℒ2β loop conformation is created by fitting the loop into the FSHR inner LRR concave surface by means of intimate hydrophobic interactions between the loop and the primary binding site of FSHR (Figs. 3*A* and 4*B*, *Inset* and Fig. S2). Therefore, the nascent FSH-binding pocket at the sTyr site is induced by binding of the hormone to $FSHR_{HB}$ rather than by the incoming sulfated tyrosine itself.

Potential Exosite for Additional FSH/FSHR Interactions. The unexpected trimeric arrangement of the FSH–$FSHR_{ED}$ complex suggests an additional hormone-receptor interaction site outside the primary recognition area (hence termed exosite) (Fig. 3*B*). This potential exosite involves the interaction of the convex surface of LRRs of FSHR with a neighboring FSH, rather than its tightly bound FSH. Each exosite buries a 610-$Å^2$ solvent-accessible surface area. Three exosites, in combination with the receptor-receptor contacts, bury a 3,850-$Å^2$ total surface area in trimer formation. Although the physiological relevance of the exosite remains to be firmly established, we describe it here to invite experimental work to examine the biological significance of the FSHR trimer because it can explain some observations that were not explainable with a monomeric complex structure. Foremost, the oligosaccharide at N52α at the edge of this site has been well known to be essential for the full agonistic activity of GPHs, because removal of the oligosaccharide dramatically reduces the efficacy of the hormones (26, 27). In hCG, this loss of efficacy attributable to N52α can be reversed by addition of an oligosaccharide at N77β in loop ℒ3β (corresponding to D71β in FSH) (11) or treatment of a monoclonal antibody (B111) that recognizes the nearby residues (11), all of which are located near the exosite. In TSH, the superagonist (TSH + α4K) can be engineered to an ultra-superagonist (TSH + α4K + β3R) when three residues in the β chain (I58β, E63β, and L69β, corresponding to V57β, R62β, and H68β in FSH) were mutated to arginines (28).

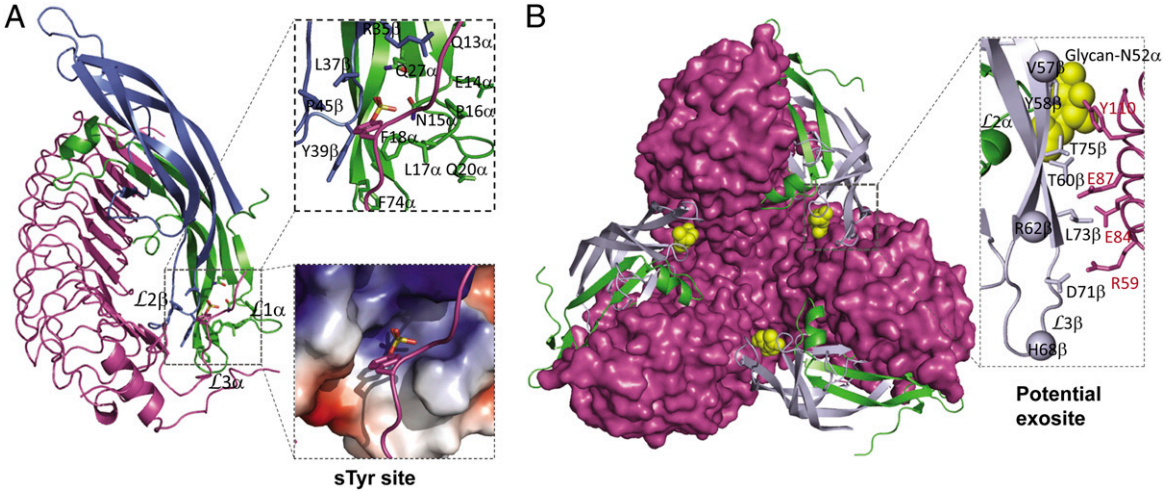

Fig. 3. Hormone-receptor interactions outside the primary binding site. (*A*) sTyr site, with close-up views of the interactions within the FSH–$FSHR_{ED}$ complex monomer (*Upper Inset*) and the electrostatic potential of the sulfated tyrosine-binding pocket (*Lower Inset*). (*B*) Potential exosite related to trimerization, with a close-up view (*Inset*) of the interactions originating from the FSH–$FSHR_{ED}$ complex oligomerizations. The receptor trimer is shown as a magenta surface. FSH is shown as ribbons: green ribbons for the α-chain and light purple ribbons for the β-chain. The FSH N52α glycan is shown as yellow balls.

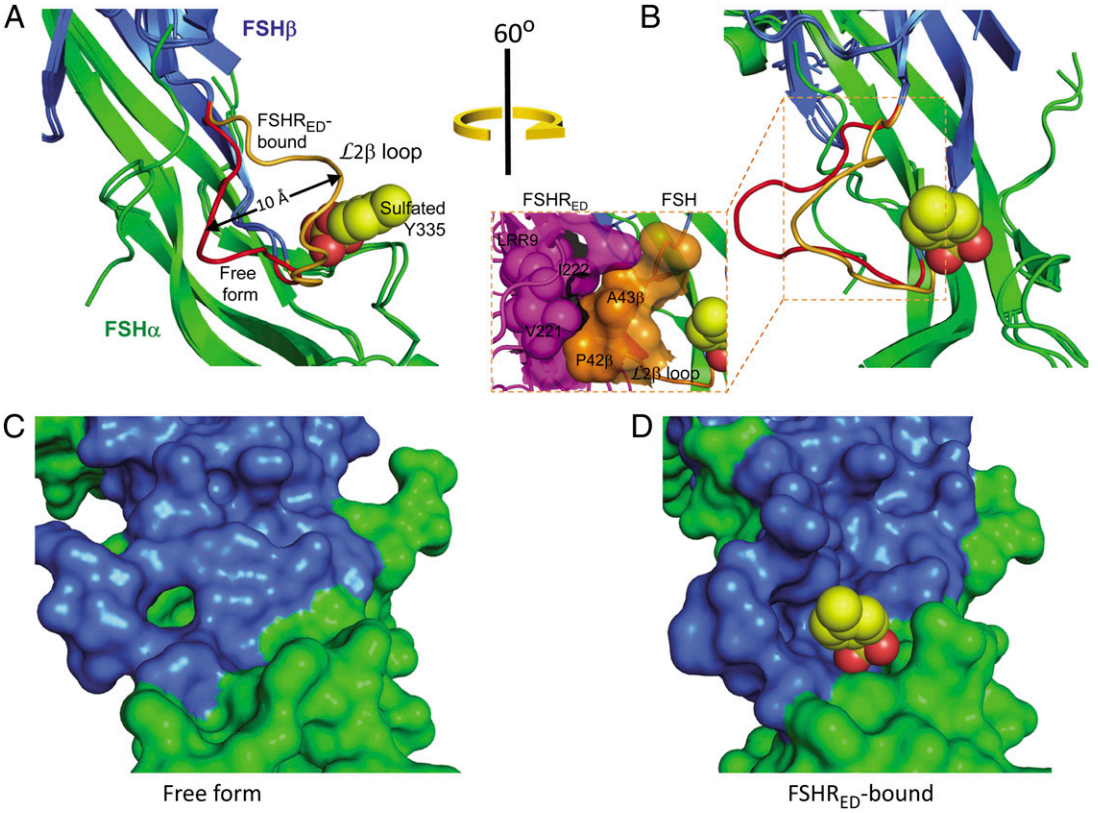

Fig. 4. Formation of the sulfate-binding pocket in FSH at the sTyr site. (*A* and *B*) Comparison of the ℒ2β loop of FSH in free form (red wire) and $FSHR_{ED}$-bound form (brown wire). FSH α-subunit is shown as green ribbons, and the rest of the β-subunit is shown as blue ribbons. Sulfated FSHR Y335 is shown as balls as a reference. The orientation of FSH in *A* and *B* is related by a rotation of 60°. Residues around A43β in the ℒ2β loop of FSH swing ∼10 Å from the free form to the $FSHR_{ED}$-bound form to form the sulfate-binding pocket. (*B*, *Inset*) Newly formed FSH pocket is structurally supported by the hydrophobic interactions between the left wall of the pocket and the FSHR residues around V221 and I222. (*C* and *D*) Surface representations show the rearrangement of the FSH ℒ2β loop on receptor binding. FSH α- and β-subunits are colored green and blue, respectively.

These TSH β3R mutations are also located at the analogous positions in the exosite. Although the potential exosite is consistent with the above functional data, its existence awaits biophysical proof of the FSHR trimer under physiological conditions.

Implications for GPHR Signaling. Our FSH–$FSHR_{ED}$ complex structure, compared with free FSH and the hormone-binding domain-only FSH–$FSHR_{HB}$ complex structures, suggests two-step FSH/FSHR recognition for initiating FSHR signaling (Fig. 5*A*). In the first step, the quiescent FSHR, designated as state (a) in Fig. 5*A*, exploits its large area of the inner concave surface of LRRs 1–8 to recruit FSH to the hormone-binding subdomain. This initial high-affinity interaction causes the FSH ℒ 2β loop to adopt the "swung-in" conformation, leading to an additional hydrophobic interaction between the ℒ 2β loop and FSHR around LRR 8/9, as well as the formation of a sTyr-binding pocket at the interface of α- and β-subunits of FSH. The end state after the recruitment step is designated as state (b) (Fig. 5*A*). In the second step, FSH uses the nascent pocket to accept the sulfated Y335 into the hole, preparing for FSHR to enter the active state (c) (Fig. 5*A*). The two-step recognition highlights the sTyr-harboring hinge region as a pivotal link in signal transduction, consistent with the functional studies that FSHR signaling is dependent on sTyr recognition (16). Given the close sequence and functional similarities between the different members of the GPH and GPHR families, this two-step recognition should be applicable to LHR and TSH receptor as well.

The docking of FSHR sTyr to the FSH pocket might accompany a conformational change of the FSHR hinge region and lead to receptor activation. Although direct evidence is unavailable, lifting the sTyr-harboring loop may unlock the inhibitory nature of the hinge region, a job that might be mimicked by the constitutive activation of FSHR mutation S273I (29), located on the helix in the hinge region preceding the sTyr-harboring loop (Fig. 2*B*, *Inset*).

As a first step to test the role of the lifting of the sTyr-harboring loop and to validate the biological significance of the sTyr site and the potential exosite, we designed two FSH mutations and tested their effects on receptor signaling. One mutation was designed to lift the sulfated Y335 of FSHR further up away from the transmembrane domain. We mutated the FSH residue F74α, which is below the sulfated tyrosine-binding pocket, to glutamate, anticipating the negative charge to enhance receptor signaling by pushing the negatively charged sulfated Y335 further toward the upper rim of the pocket (Fig. 5*B*). As shown in Fig. 5*C*, the FSH αF74E mutation enhances signaling by ∼70% in β-arrestin activity assay or ∼65% in the estradiol production assay, as measured by maximum receptor response. Note that the ligand potency was not increased, suggesting high signaling efficiency is not correlated with potency. Another mutation, βL73E, was designed at the potential exosite. As shown in Fig. 5*C*, this mutation enhances signaling by ∼85% in β-arrestin activity assay or ∼70% in the estradiol production assay over the WT without increasing potency. Together, these data support that lifting the sTyr-harboring loop may be functionally important and that both the sTyr site and the potential exosite can be used to modulate FSHR signaling, which may shed light on the direction of drug development for treatment of GHPR-related diseases. Future work should be directed to define the conformational change of the FSHR hinge region on

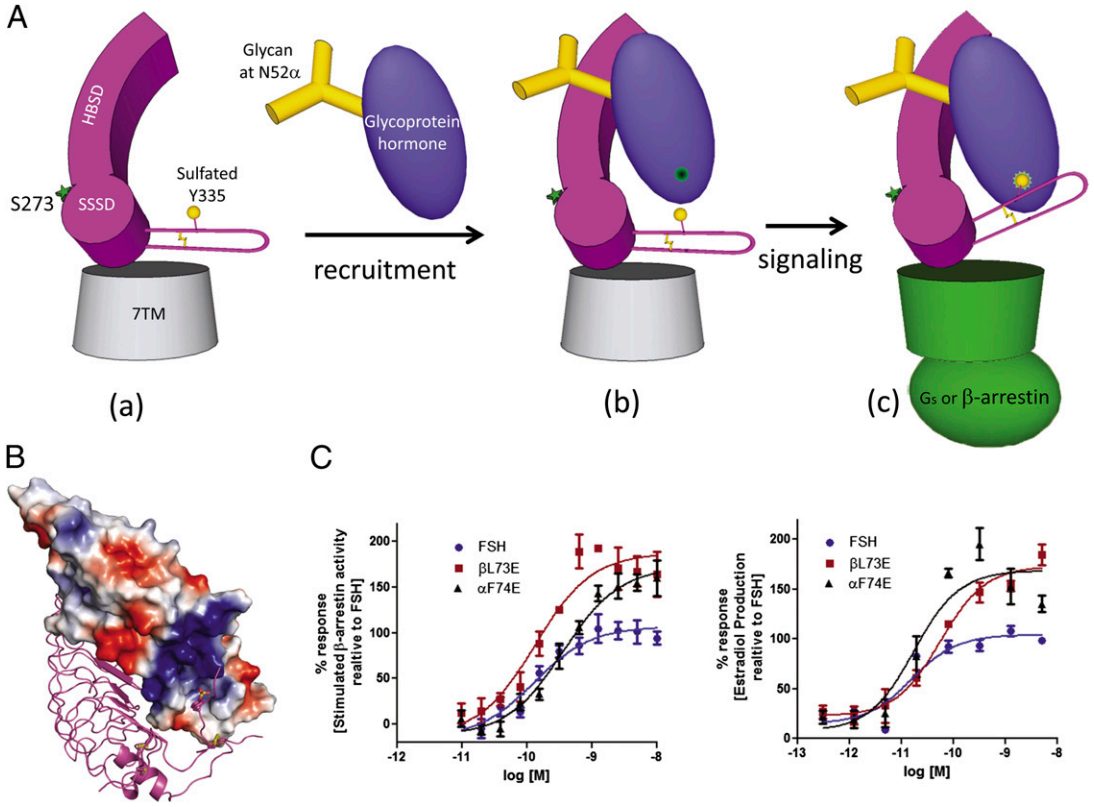

Fig. 5. Two-step FSH/FSHR recognition and functional validations of the sTyr site and the exosite. (*A*) Schematic diagram of the two-step recognition. The GPHR's extracellular LRRs, in a putative orientation relative to the seven-transmembrane (7TM) domain, are shown as magenta blocks with the flexible loop as a hairpin, and the 7TM domain is shown as cylinders with the inactivated state colored gray and the activated state colored green. The hormone-binding subdomain is labeled as HBSD, and signal specificity subdomain is labeled as SSSD. Sulfated Y335 is shown as yellow balls, residue S271 is shown as green stars, and disulfide bonds are shown as brown sticks. Heterotrimeric G_s or β-arrestin protein is shown as a green ellipsoid. GPH heterodimer is represented in purple, whereas carbohydrates at N52α are shown as a yellow Y-shaped stick. Shown here is only one of the possible orientations of the extracellular domain relative to the 7TM domain. (*B*) Importance of electrostatic potential of FSH in lifting the Y335-harboring FSHR hairpin for receptor activation. Negative potential is colored red, and positive potential is colored blue. $FSHR_{ED}$ is represented as magenta ribbons, with the side chain of sulfated Y335 shown as sticks. (*C*) Validation of the roles of the sTyr site and the exosite in FSHR activation by FSH mutagenesis. (*Left*) Relative amount of β-arrestin recruited for binding to the activated FSHR inside the CHO cell on stimulation by FSH or its mutants. The amount of recruited β-arrestin is normalized to 100% for the maximum response of FSH. Data represent experiments performed with quadruplicate samples. (*Right*) Relative amount of estradiol production inside primary granulosa cells from immature rats on stimulation by FSH or its mutants. The amount of estradiol production is normalized to 100% for the maximum response of FSH. Data represent experiments performed with triplicate samples.

sTyr recognition, as well as the specific mechanism entailing the potential exosite for FSH/FSHR interactions.

Experimental Procedures

Cell Culture, Cloning, and Baculovirus-Mediated Mammalian Cell Gene Transduction Expression. Sf9 insect cells were maintained in SF900-II media (Invitrogen) supplemented with 8% (vol/vol) heat-inactivated FBS. *N*-acetylglucosaminyltransferase-deficient (GnTI$^-$) HEK293 cells were maintained in CDM4HEK293 media (HyClone) supplemented with 4% (vol/vol) heat-inactivated FBS. To construct the single-chain FSH, we joined the FSHB coding sequence (N1-G122) and the common glycoprotein hormone alpha chain (CGA) coding sequence (A1-S92) with a GGGSGGNSGGGSGGGS linker, generally following the scheme described previously (8). This joined DNA fragment and the cDNA fragment encoding the full ectodomain of human $FSHR_{ED}$ (S16-R366) were attached to an N-terminal Gaussian luciferase signal peptide and a C-terminal 7-histidine tag, and were then subcloned into the baculovirus-mediated mammalian cell gene transduction (BacMam) vector pVLAD6 (30). The constructs and the BacVector-3000 baculovirus DNA (EMD Chemicals) were used to cotransfect Sf9 cells in six-well plates in the presence of the Insect GeneJuice reagent (EMD Chemicals). After incubation of the transfected cells at 27 °C for 5 d, the resulting low-titer virus stock was harvested and used to infect Sf9 cells at 2×10^6 cells/mL for amplification. The amplified BacMam viruses were used to coinfect 20 L of GnTI$^-$ HEK293 cells at a density of 1.5×10^6 cells/mL. The cells were pelleted 72 h later, and the supernatants were concentrated and buffer-exchanged to HBS [10 mM Hepes (pH 7.5), 150 mM NaCl]. The recombinant proteins were captured by the Talon affinity resin and eluted with 300 mM imidazole (pH 7.5), glycan-minimized with endoglycosidase-F1 (Sigma), and treated with bovine carboxypeptidase-A (Sigma) for His-tag removal. The proteins were further purified with size exclusion columns (Superdex-200; Amersham Biosciences) preequilibrated and eluted with HBS. The FSH mutants were constructed using overlap extension PCR, based on the above WT single-chain FSH construct. Subcloning, baculovirus generation, protein expression, and purification of these mutants were performed using the same protocols for the WT.

Crystallization and Data Collection. The glycan-minimized FSH–$FSHR_{ED}$ complex was concentrated by ultrafiltration to about 10 mg/mL in HBS. The crystals were grown using hanging-drop vapor diffusion at 20 °C by mixing equal volumes of the purified protein and the crystallization condition of 0.1 M Hepes (pH 7.5), 10% (vol/vol) isopropanol, and 20% (wt/vol) polyethylene glycol 4000. For data collection, crystals were flash-frozen in the respective crystallization conditions supplemented with 15% (vol/vol) ethylene glycol. Diffraction data were collected at the 21-ID-D beam line of the Advanced Photon Source. Diffraction data were processed using the HKL3000 suite (31), and their statistics are shown in Table S1.

Structure Determination and Refinement. The structure was solved by molecular replacement with PHASER in CCP4 (32) using the FSH–$FSHR_{HB}$ complex (Protein Data Bank ID code 1XWD) as the search model. Initial models were

subjected to rigid-body refinement followed by positional and simulated-annealing refinements using CNS (33). Reiterated cycles of model building and refinement were carried out using O (34), REFMAC with TLS parameterization (35), and PHENIX (36). A tight geometry and threefold noncrystallographic symmetry (NCS) restraints had been incorporated throughout the refinement process until the last two refinement cycles. The structure was analyzed using the CCP4 suite (32), and the figures were made using PyMOL (37).

FSHR β-Arrestin Recruitment Assay. Determination of activated FSHR was performed by measuring β-arrestin recruitment according to the PathHunter FSHR β-arrestin assay protocol (DiscoveRx). CHO-K1 cells stably coexpressing both ProLink-tagged FSHR and β-galactosidase–tagged β-arrestin fusion proteins were seeded into 384-well microplates at a density of 5,000 cells per well and were allowed to adhere overnight before compound addition. For each assay, cells were incubated at 37 °C for 90 min in the presence of glycosylated FSH or mutants. After incubation, chemiluminescent signal from activated β-galactosidase enzyme was generated through the addition of 15 μL (50% vol/vol) of PathHunter Detection reagent mixture (DiscoveRx), followed by incubation for 1 h at room temperature. Microplates were read with a PerkinElmer Envision instrument for chemiluminescent signal detection. Data were analyzed using GraphPad Prism software.

Primary Granulosa Isolation and Determination of Estradiol Production. Primary granulosa cells from immature rats were used to determine the ability of FSH and its mutants to induce aromatase and synthesize estradiol from its precursor androstenedione. All the animal protocols were carried out in accordance with institutional animal care and use committee recommendations and the institutional ethical committee (EMD Serono Research Institute) (38). Briefly, 21-d-old female CD rats (obtained from Charles River Laboratory) were implanted with diethylstilbestrol pellets (1-mg release for 7 d; Innovative Research of America), and 72 h after implantation, the rats were euthanized and ovaries were harvested. The ovaries were crushed to release the granulosa cells in DMEM/F12 (Invitrogen), which contains 5% FBS and antibiotics. The cell suspension was filtered and washed to obtain granulosa cells. The isolated granulosa cells were cultured in a 96-well plate overnight at 37 °C in DMEM/F12 that contains serum. On the following day, the cells were treated with serially diluted FSH in serum-free DMEM/F12 that contains 0.1% BSA and androstenedione (10^{-7} M). After 24 h of incubation, the medium was collected and the estradiol in the medium was determined by ELISA (DRG). The obtained estradiol values were plotted and analyzed using Prism software.

ACKNOWLEDGMENTS. We thank M. Muda, P. Stein, R. Campbell, S. Palmer, S. McKenna, M. Frech, S. Nataraja, C. Kelton, Z. Luo, I. Mochalkin, and D. Musil for helpful discussions.

1. Pierce KL, Premont RT, Lefkowitz RJ (2002) Seven-transmembrane receptors. *Nat Rev Mol Cell Biol* 3:639–650.
2. Simoni M, Gromoll J, Nieschlag E (1997) The follicle-stimulating hormone receptor: Biochemistry, molecular biology, physiology, and pathophysiology. *Endocr Rev* 18: 739–773.
3. Ulloa-Aguirre A, Zariñán T, Pasapera AM, Casas-González P, Dias JA (2007) Multiple facets of follicle-stimulating hormone receptor function. *Endocrine* 32:251–263.
4. Tao YX, Segaloff DL (2009) Follicle stimulating hormone receptor mutations and reproductive disorders. *Prog Mol Biol Transl Sci* 89:115–131.
5. Wu H, Lustbader JW, Liu Y, Canfield RE, Hendrickson WA (1994) Structure of human chorionic gonadotropin at 2.6 A resolution from MAD analysis of the selenomethionyl protein. *Structure* 2:545–558.
6. Lapthorn AJ, et al. (1994) Crystal structure of human chorionic gonadotropin. *Nature* 369:455–461.
7. Fox KM, Dias JA, Van Roey P (2001) Three-dimensional structure of human follicle-stimulating hormone. *Mol Endocrinol* 15:378–389.
8. Fan QR, Hendrickson WA (2005) Structure of human follicle-stimulating hormone in complex with its receptor. *Nature* 433:269–277.
9. Moyle WR, et al. (1994) Co-evolution of ligand-receptor pairs. *Nature* 368:251–255.
10. Braun T, Schofield PR, Sprengel R (1991) Amino-terminal leucine-rich repeats in gonadotropin receptors determine hormone selectivity. *EMBO J* 10:1885–1890.
11. Moyle WR, et al. (2004) Model of glycoprotein hormone receptor ligand binding and signaling. *J Biol Chem* 279:44442–44459.
12. Mueller S, Jaeschke H, Günther R, Paschke R (2010) The hinge region: An important receptor component for GPHR function. *Trends Endocrinol Metab* 21:111–122.
13. Jiang X, et al. (1995) Structural predictions for the ligand-binding region of glycoprotein hormone receptors and the nature of hormone-receptor interactions. *Structure* 3:1341–1353.
14. Fan QR, Hendrickson WA (2007) Assembly and structural characterization of an authentic complex between human follicle stimulating hormone and a hormone-binding ectodomain of its receptor. *Mol Cell Endocrinol* 260–262:73–82.
15. Moyle WR, et al. (2005) Models of glycoprotein hormone receptor interaction. *Endocrine* 26:189–205.
16. Costagliola S, et al. (2002) Tyrosine sulfation is required for agonist recognition by glycoprotein hormone receptors. *EMBO J* 21:504–513.
17. Zhang M, et al. (2000) The extracellular domain suppresses constitutive activity of the transmembrane domain of the human TSH receptor: Implications for hormone-receptor interaction and antagonist design. *Endocrinology* 141:3514–3517.
18. Ji I, Lee C, Song Y, Conn PM, Ji TH (2002) Cis- and trans-activation of hormone receptors: The LH receptor. *Mol Endocrinol* 16:1299–1308.
19. Kajava AV (1998) Structural diversity of leucine-rich repeat proteins. *J Mol Biol* 277: 519–527.
20. Koo YB, Ji I, Slaughter RG, Ji TH (1991) Structure of the luteinizing hormone receptor gene and multiple exons of the coding sequence. *Endocrinology* 128:2297–2308.
21. Gromoll J, Pekel E, Nieschlag E (1996) The structure and organization of the human follicle-stimulating hormone receptor (FSHR) gene. *Genomics* 35:308–311.
22. Bruysters M, Verhoef-Post M, Themmen AP (2008) Asp330 and Tyr331 in the C-terminal cysteine-rich region of the luteinizing hormone receptor are key residues in hormone-induced receptor activation. *J Biol Chem* 283:25821–25828.
23. Bonomi M, Busnelli M, Persani L, Vassart G, Costagliola S (2006) Structural differences in the hinge region of the glycoprotein hormone receptors: Evidence from the sulfated tyrosine residues. *Mol Endocrinol* 20:3351–3363.
24. Lindau-Shepard B, Brumberg HA, Peterson AJ, Dias JA (2001) Reversible immunoneutralization of human follitropin receptor. *J Reprod Immunol* 49(1):1–19.
25. Szkudlinski MW, Teh NG, Grossmann M, Tropea JE, Weintraub BD (1996) Engineering human glycoprotein hormone superactive analogues. *Nat Biotechnol* 14:1257–1263.
26. Matzuk MM, Keene JL, Boime I (1989) Site specificity of the chorionic gonadotropin N-linked oligosaccharides in signal transduction. *J Biol Chem* 264:2409–2414.
27. Flack MR, Froehlich J, Bennet AP, Anasti J, Nisula BC (1994) Site-directed mutagenesis defines the individual roles of the glycosylation sites on follicle-stimulating hormone. *J Biol Chem* 269:14015–14020.
28. Grossmann M, Leitolf H, Weintraub BD, Szkudlinski MW (1998) A rational design strategy for protein hormone superagonists. *Nat Biotechnol* 16:871–875.
29. Nakabayashi K, Kudo M, Kobilka B, Hsueh AJ (2000) Activation of the luteinizing hormone receptor following substitution of Ser-277 with selective hydrophobic residues in the ectodomain hinge region. *J Biol Chem* 275:30264–30271.
30. Dukkipati A, Park HH, Waghray D, Fischer S, Garcia KC (2008) BacMam system for high-level expression of recombinant soluble and membrane glycoproteins for structural studies. *Protein Expr Purif* 62(2):160–170.
31. Otwinowski ZM, Minor W (1997) Processing of X-ray diffraction data collected in oscillation mode. *Methods Enzymol* 276:307–326.
32. Collaborative Computational Project, Number 4 (1994) The CCP4 suite: Programs for protein crystallography. *Acta Crystallogr D Biol Crystallogr* 50:760–763.
33. Brünger AT, Adams PD, Rice LM (1998) Recent developments for the efficient crystallographic refinement of macromolecular structures. *Curr Opin Struct Biol* 8: 606–611.
34. Jones TA, Zou JY, Cowan SW, Kjeldgaard M (1991) Improved methods for building protein models in electron density maps and the location of errors in these models. *Acta Crystallogr A* 47(2):110–119.
35. Winn MD, Murshudov GN, Papiz MZ (2003) Macromolecular TLS refinement in REFMAC at moderate resolutions. *Methods Enzymol* 374:300–321.
36. Adams PD, et al. (2010) PHENIX: A comprehensive Python-based system for macromolecular structure solution. *Acta Crystallogr D Biol Crystallogr* 66:213–221.
37. DeLano WL (2002) The PyMOL Molecular Graphics System (DeLano Scientific LLC, San Carlos, CA).
38. Sriraman V, Sharma SC, Richards JS (2003) Transactivation of the progesterone receptor gene in granulosa cells: Evidence that Sp1/Sp3 binding sites in the proximal promoter play a key role in luteinizing hormone inducibility. *Mol Endocrinol* 17: 436–449.